


## Turbulence Transition in Magnetically Confined Hydrogen and Deuterium Plasmas

T. Kinoshita<sup>1</sup>, K. Tanaka<sup>2,3</sup>, A. Ishizawa<sup>4</sup>, H. Sakai<sup>2</sup>, M. Nunami<sup>3,5</sup>, Y. Ohtani<sup>6</sup>, H. Yamada<sup>7</sup>, M. Sato<sup>3</sup>,  
 M. Nakata<sup>3,8</sup>, T. Tokuzawa<sup>3,8</sup>, R. Yasuhara<sup>3,8</sup>, Y. Takemura<sup>3,8</sup>, I. Yamada<sup>3</sup>, H. Funaba<sup>3</sup>, K. Ida<sup>3,8</sup>,  
 M. Yoshinuma<sup>3,8</sup>, T. Tsujimura<sup>3,8</sup>, R. Seki<sup>3,8</sup>, K. Ichiguchi<sup>3,8</sup> and C. A. Michael<sup>9</sup>

<sup>1</sup>Research Institute for Applied Mechanics, Kyushu University, Kasuga, Fukuoka 816-8580, Japan  
<sup>2</sup>Interdisciplinary Graduate School of Engineering Sciences, Kyushu University, Kasuga, Fukuoka 816-8580, Japan  
<sup>3</sup>National Institute for Fusion Science, National Institutes on Natural Sciences, Toki, Gifu, 509-5292, Japan  
<sup>4</sup>Graduate School of Energy Science, Kyoto University, Uji, Kyoto, 611-0011, Japan  
<sup>5</sup>Graduate School of Science, Nagoya University, Nagoya, Aichi, 464-8601, Japan  
<sup>6</sup>National Institutes for Quantum and Radiological Science and Technology, Naka, Ibaraki, 311-0193, Japan  
<sup>7</sup>Graduate School of Frontier Sciences, The University of Tokyo, Kashiwa, Chiba 277-8568, Japan  
<sup>8</sup>The Graduate University for Advanced Studies, SOKENDAI, Toki, Gifu, 509-5292, Japan  
<sup>9</sup>Department of Physics and Astronomy, University of California - Los Angeles, Los Angeles, California 90095-7099, USA

 (Received 12 June 2022; revised 29 May 2023; accepted 4 March 2024; published 7 June 2024)

In this study, we discovered a turbulence transition in a large helical device. The turbulence level and turbulence-driven energy transport decrease to a specific transition density and increase above it. The ruling turbulences below and above the transition density were ion-temperature gradient (ITG) and resistive-interchange (RI) turbulences, consistent with the predictions of gyrokinetic theory and two-fluid MHD model, respectively. Isotope experiments on hydrogen (H) and deuterium (D) clarified the role of transitions. In the ITG regime, turbulence levels and energy transport were comparable in the H and D plasmas. In contrast, in the RI regime, they were clearly suppressed in the D plasma. The results provide crucial knowledge for understanding isotope effects and future optimization of stellarator and heliotron devices.

DOI: [10.1103/PhysRevLett.132.235101](https://doi.org/10.1103/PhysRevLett.132.235101)

Nuclear fusion reactors with magnetically confined plasmas are attractive future energy sources. Tokamaks are currently the most advanced device concept, and stellarators and heliotrons are an alternative concept with the advantage of steady-state operation without a plasma-current drive. In tokamaks, transport is dominated by turbulence-driven anomalous processes. On the other hand, in stellarators and heliotrons, neoclassical transport is also essential because of the three-dimensional magnetic configuration. In these toroidal devices, the dominant ion-scale turbulence varies and transits depending on the plasma parameters. For instance, in a linear theory, the increase of scale length ratio of density to ion temperature gradient destabilizes ion temperature gradient (ITG) turbulence, whereas it stabilizes the trapped electron mode (TEM) turbulence [1]. The turbulence transition affects the transport characteristics such as energy [2], particle [3], and momentum transport [2,4].

The large helical device (LHD) [5] is one of the largest stellarator and heliotron devices. Comparing with advanced

stellarators such as the Wendelstein 7-X [6], the magnetic configuration is not optimized to reduce neoclassical transport, and the contribution of neoclassical transport is larger [7,8]. In addition, turbulence-driven transport is also not negligible in LHD [8–10], thus, it is essential to investigate the underlying physics of anomalous transport in stellarators and heliotrons as well as in tokamaks. In the core region of LHD, density gradient-driven TEM cannot be unstable because of the flat or hollow density profiles due to the neoclassical thermodiffusion [11]. Therefore, ITG is the dominant instability in most cases [12–15]. In addition to drift-wave instabilities, interchange modes become unstable owing to a magnetic-hill configuration in LHD [16]. To suppress ideal interchange modes, the magnetic configuration is designed to have a strong magnetic shear, however, is not able to stabilize resistive interchange (RI) modes [17]. RIs with low-poloidal and toroidal modes in high- $\beta$  plasmas have been extensively studied for avoiding the internal collapse event that limits the achievable  $\beta$  [18], and high-poloidal and toroidal modes have been shown to affect energy transport [19,20]. However, the role of high-mode resistive-interchange (RI) turbulence in the transport of low- $\beta$  plasmas is not understood, and the relation to ITG-driven transport is of great interest. Thus, an investigation of ITG and RI turbulences in LHD will shed new light on the physics of turbulence in

---

*Published by the American Physical Society under the terms of the Creative Commons Attribution 4.0 International license. Further distribution of this work must maintain attribution to the author(s) and the published article's title, journal citation, and DOI.*

toroidal devices and be valuable for the future configuration and optimization of stellarators and heliotrons.

Herein, we conducted two experiments to comprehensively understand turbulence-driven transport in LHD and discovered a transition from ITG turbulence to RI turbulence. One is a density ramp-up experiment to demonstrate the presence of turbulence transitions, and the other is a shot-by-shot density scan experiment to clarify the relationship between turbulence and transport through mode identification. The shot-by-shot density scan experiments were conducted in H and D plasmas to further understand the turbulence transition. These experiments were conducted in an inward-shifted configuration with the magnetic axis position ( $R_{ax}$ ) at 3.6 m and the toroidal magnetic field ( $B_t$ ) at 2.75 T. This configuration shows the best performance in LHD and is the most widely used [21]. Figure 1 shows the turbulence behavior in a density ramp-up experiment [shot No. 143757(H)]. In this experiment, the line-averaged electron density  $\bar{n}_e$  was ramped up from  $1 \times 10^{19}$  to  $3.5 \times 10^{19} \text{ m}^{-3}$  in 2.5 MW ECRH H plasma. Figure 1(b) shows the time evolution of the turbulence level  $\bar{n}_e/n_e$  (i.e., the local turbulence amplitude  $\bar{n}_e$  normalized by the local electron density  $n_e$ ). We measured the turbulence using two-dimensional phase contrast imaging (2D-PCI), which measures the poloidal-dominated wave numbers  $k = 0.1\text{--}0.8 \text{ mm}^{-1}$  over the frequency range  $f = 32\text{--}500 \text{ kHz}$  [22–24] corresponding to the ion-scale turbulence. The white area in Fig. 1(b), which appears as a valley, corresponds to the area with the lowest turbulence level. The turbulence level first decreases with an increase in density over time; however, after reaching the minimum value, it increases with further increasing density. Simultaneously, its propagation direction switched from the ion-diamagnetic (i-dia.) direction toward the electron-diamagnetic (e-dia.) direction in the laboratory frame. These results show that different turbulence

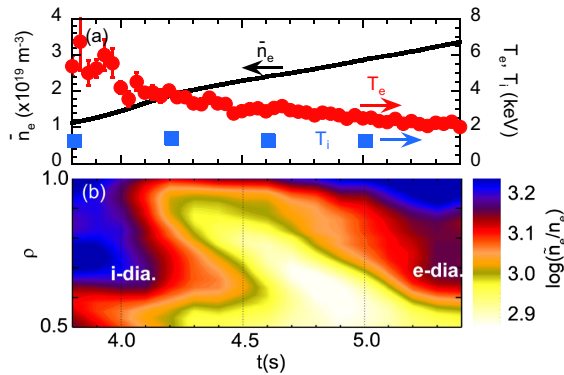


FIG. 1. Time evolution of (a) the line-averaged electron density  $\bar{n}_e$  and the central electron and ion temperatures,  $T_e$  and  $T_i$ , respectively. (b) Ion-scale turbulence level profile in the density ramp-up experiment using hydrogen plasma. Here,  $\rho$  is the radius normalized by the averaged minor radius, which includes 99% electron kinetic energy [25].

modes appear in different density regimes under identical heating conditions.

To understand the turbulence transition and its role in transport, we conducted shot-by-shot density-scan experiments [48 successful shots from No. 160120-160170(H), 45 successful shots from No. 157143-157186(D)]. Two 154-GHz microwaves for heating were injected tangentially co and counter to  $B_t$  to cancel out the EC-driven current. The total ECRH power was adjusted to 1.4 MW in the H and D plasmas. The purities of H and D plasmas were more than 90%. Figures 2(a) and 2(b) show the density dependence of the turbulence level  $\bar{n}_e/n_e$  and its phase velocity in the laboratory frame  $V_{lab}$  measured by 2D-PCI. These are averaged values for the range of normalized radii  $\rho = 0.5\text{--}0.7$ , as the turbulence changes during the series of experiments. Figure 2(a) shows that the turbulence level first decreases with increasing  $\bar{n}_e$ , and after reaching a minimum value, it increases with further increasing  $\bar{n}_e$ . This density dependence of  $\bar{n}_e/n_e$  is also observed in the density ramp-up experiment [Fig. 1(b)]. We define the transition density ( $n_{tr}$ ) to be the density at which the turbulence level reaches a minimum value, as indicated by the dashed lines in Fig. 2. The transition density is  $1.6 \times 10^{19}$  and  $2.6 \times 10^{19} \text{ m}^{-3}$  in the H and D plasmas, respectively. The turbulence levels are comparable in the H and D plasmas for  $\bar{n}_e < n_{tr}$ , whereas it is lower in the D plasma than in the H plasma for  $\bar{n}_e > n_{tr}$ . As shown in Fig. 2(b), the turbulence propagates in the i-dia. direction for  $\bar{n}_e < n_{tr}$  and in the e-dia. direction for  $\bar{n}_e > n_{tr}$  in the laboratory frame. The reversed density dependence of the turbulence level, the turbulence suppression in the D plasma only for  $\bar{n}_e > n_{tr}$  and the different propagation directions strongly suggest that the dominant turbulence modes are different in each density regime.

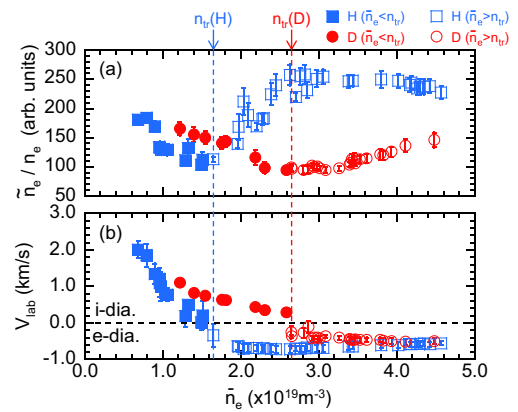


FIG. 2. Electron-density dependence of (a) the turbulence level and (b) phase velocity of turbulence in the laboratory frame.  $n_{tr}(H)$  and  $n_{tr}(D)$  represent the transition densities in the H and D plasmas, respectively. The blue and red symbols represent the H and D plasmas, respectively. The closed and open symbols represent  $\bar{n}_e < n_{tr}$  and  $\bar{n}_e > n_{tr}$ , respectively. The values are averaged at  $\rho = 0.5\text{--}0.7$ .

To discuss the role of the observed turbulence on the confinement characteristic, the density dependence of the global energy confinement time ( $\tau_E$ ) and the anomalous contributions to the electron and ion thermal conductivities are shown in Fig. 3. Figure 3(a) shows that the density dependence of  $\tau_E$  changes at  $n_{tr}$ , becoming more weakly positive for  $\bar{n}_e > n_{tr}$ . The global energy-confinement time is almost identical in the H and D plasmas for  $\bar{n}_e < n_{tr}$ , whereas  $\tau_E$  is extended in the D plasma for  $\bar{n}_e > n_{tr}$ . Figures 3(b) and 3(c) show the density dependence of the anomalous thermal conductivity of ion and electron. We evaluated the anomalous thermal conductivities by subtracting the neoclassical conductivities from the experimental conductivities ( $\chi_{e,i,ano} = \chi_{e,i,exp} - \chi_{e,i,neo}$ ). The experimental conductivities were obtained from a power-balance analysis using LHDGAUSS [26] and TASK3D [27], and the neoclassical conductivities using GSRAKE [28]. Some of the datasets in the high-density regime were omitted because the electron and ion temperatures are close, which makes it difficult to evaluate the electron and ion thermal conductivities separately. As shown in Fig. 3(b), in the low-density regime,  $\chi_{e,ano}$  decreases as  $\bar{n}_e$  increases, and the values are almost identical in the H and D plasmas. This is qualitatively consistent with the  $\bar{n}_e$  dependence of the turbulence level shown in Fig. 2(a). Simultaneously,  $\chi_{i,ano}$  is close to zero, suggesting that ion transport is dominated by neoclassical transport in this regime. Thus, the correspondence between the turbulence levels and  $\chi_{e,ano}$  suggests that ion-scale turbulence plays a role in electron-energy transport in

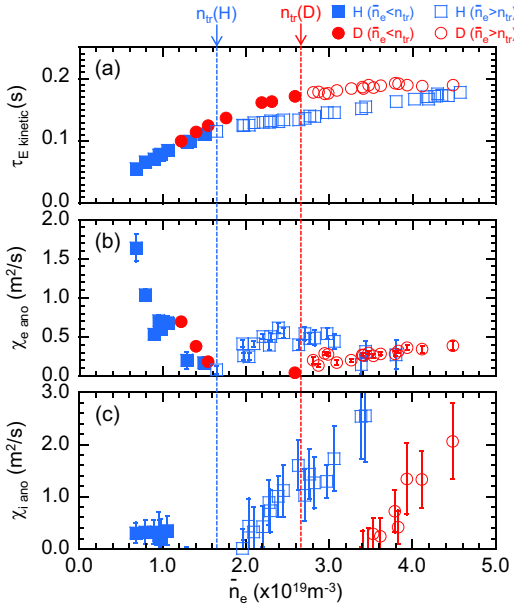


FIG. 3. Electron-density dependence of (a) global kinetic energy-confinement time, (b) anomalous electron thermal conductivity, and (c) anomalous ion thermal conductivity. The values in (b) and (c) are averaged at  $\rho = 0.5\text{--}0.7$ .

the low-density regime at  $\bar{n}_e < n_{tr}$ . Meanwhile, in the high-density regime,  $\chi_{e,ano}$  and  $\chi_{i,ano}$  increase as  $\bar{n}_e$  increases in the H and D plasmas and are lower in the D plasma; this density dependence and isotope effects correspond to the turbulence level, suggesting that the measured turbulence plays an essential role in electron- and ion-energy transport.

Next, the types of turbulence above and below  $n_{tr}$  were identified by experimental parameter dependencies and linear calculations. As the electron density increases, the plasma parameters vary as follows: The electron temperature decreases, and the temperature ratio ( $T_i/T_e$ ) increases because the change in  $T_i$  is smaller than the decrease in  $T_e$ . Collisionality,  $\beta$  and plasma resistivity ( $\eta \propto T_e^{-3/2}$ ) also increase with density. The normalized  $T_e$  gradient ( $L_{T_e}^{-1} = -1/T_e dT_e/dr$ ) decreases, whereas the normalized  $T_i$  gradient ( $L_{T_i}^{-1} = -1/T_i dT_i/dr$ ) remains nearly constant. The normalized  $n_e$  gradient ( $L_{n_e}^{-1} = -1/n_e dn_e/dr$ ) decreases with increasing  $\bar{n}_e$  at  $\bar{n}_e < n_{tr}$ , and increases at  $\bar{n}_e > n_{tr}$ . Among these parameters, the normalized gradients do not play a crucial role in turbulence transitions, instead,  $T_i/T_e$  and  $\eta$  are clear indicators of turbulence identification. As shown in Figs. 4(a) and 4(b), the turbulence level decreases with increasing  $T_i/T_e$  and  $\eta$  in  $\bar{n}_e < n_{tr}$  and increases in  $\bar{n}_e > n_{tr}$  in the H and D plasmas. In other words,  $T_i/T_e$  and/or  $\eta$  are stabilizing terms for turbulence at  $\bar{n}_e < n_{tr}$  and destabilizing terms at  $\bar{n}_e > n_{tr}$ . These results suggest that the turbulence mode differs at each density regime.

For further investigation, we performed linear calculations of the instabilities. First, gyrokinetic linear calculations were carried out by using the local flux-tube gyrokinetic simulation code (GKV) [29,30] including the kinetic electrons, collisionality, and electromagnetic effects. In our linear analysis, grid points of 480, 32, and 15 in the coordinate along the field line  $z$ , parallel velocity  $v_{\parallel}$ ,

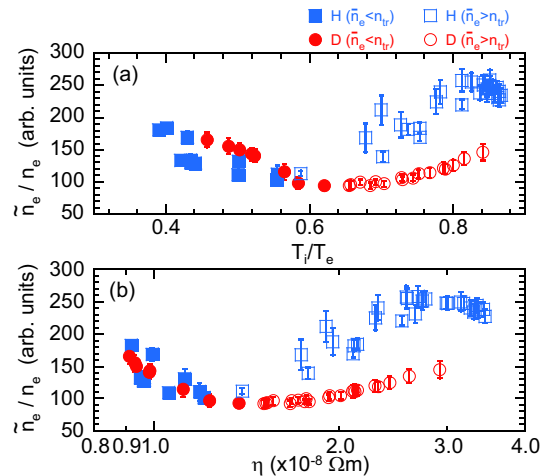


FIG. 4. Dependence of turbulence level on (a) ion-electron temperature ratio, (b) plasma resistivity averaged at  $\rho = 0.5\text{--}0.7$ .

and perpendicular velocity  $v_{\perp}$  directions are distributed in  $-10\pi \leq z \leq 10\pi$ ,  $-4v_{Ts} \leq v_{\parallel} \leq 4v_{Ts}$ , and  $0 \leq v_{\perp} \leq 4v_{Ts}$ , respectively. The wavenumber in the Fourier space is represented by  $k_x=0$  and  $k_y\rho_i=0.1 \times m$ , where  $1 \leq m \leq 10$ , corresponding to the measurement region of 2D-PCI. The effect of impurities on the growth rate was tested in several cases, however, the effect was negligibly small and therefore not included in these calculations.

Figure 5(a) shows the density dependence of the linear growth rates of ITG turbulence ( $\gamma_{ITG}$ ). The calculations were performed at  $\rho = 0.5, 0.6, \text{ and } 0.7$ , and the maximum values of  $\gamma_{ITG}$  are plotted. In all calculations, the real frequency is in the i-dia. direction, indicating ITG turbulence. The linear growth rate decreases with an increase in  $\bar{n}_e$  in the H and D plasmas. The reduction of  $\gamma_{ITG}$  is due to the stabilization effects of  $T_i/T_e$  and/or collisions. Meanwhile, finite- $\beta$  stabilization effects are negligible with strong magnetic shear in LHD [31]. For  $\bar{n}_e < n_{tr}$ , the reduction of  $\gamma_{ITG}$  with increasing  $\bar{n}_e$  confirms qualitatively with the decrease in the turbulence level. Furthermore, the i-dia. propagation direction in the laboratory frame is consistent with the characteristics of ITG turbulence. It is remarked that the propagation velocity of the ITG turbulence at the laboratory frame can be influenced by the  $E \times B$  flow velocity, which is not available in this series of experiments. For  $\bar{n}_e > n_{tr}$ , the linear calculation of GKV does not account for the increase in the observed turbulence level. GKV can handle TEM and microtearing modes, which are ion-scale turbulence propagating in the e-dia. direction, and thus these are ruled out. For these reasons, we conclude that non-drift-wave-type instabilities are responsible for the turbulence observed at  $\bar{n}_e > n_{tr}$ , and focus on RI turbulence due of the formation of a magnetic hill in LHD as the most promising candidate. Present GKV is unable to handle RI turbulence, which is a non-drift-wave-type instability with the parallel wavenumber  $k_{\parallel} = 0$ .

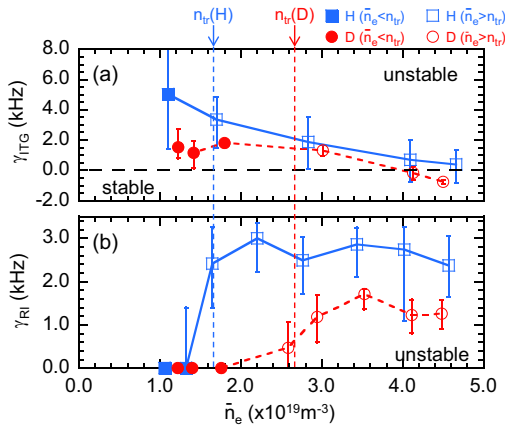


FIG. 5. Electron-density dependence of the linear growth rate of (a) ITG turbulence ( $\gamma_{ITG}$ ) and (b) RI turbulence ( $\gamma_{RI}$ ). The errors in  $\gamma_{ITG}$  and  $\gamma_{RI}$  were evaluated by changing the normalized ion temperature gradient and pressure gradient by 20%, respectively.

Therefore, we employed two-fluid MHD simulations to evaluate the growth rate of RI turbulence ( $\gamma_{RI}$ ) [32,33]. This simulation was conducted at  $\rho = 0.55$ , where a turbulence peak was observed in the experiment. As shown in Fig. 5(b), the linear growth rate of RI turbulence indicates that RI turbulence is stable for  $\bar{n}_e < n_{tr}$  in the H and D plasmas; however, both plasmas become unstable at  $\bar{n}_e > n_{tr}$ . This density dependence at  $\bar{n}_e > n_{tr}$  is consistent with the turbulence level. Moreover, a lower  $\gamma_{RI}$  in the D plasma is also consistent with a lower turbulence level, which can be interpreted for the following reasons. A linear growth rate of RI turbulence is expressed as  $\gamma_{RI} \propto \eta^{1/3} (dP/dr)^{2/3} m^{-1/3}$  ( $P$ : total pressure,  $m$ : ion mass) in the analytical solution [34]. First,  $\eta$  is lower in the D plasma because of the higher  $T_e$ . The higher  $T_e$  is formed partially due to lower electron thermal conductivity [Fig. 3(b)], and partially due to the negative ion mass dependence of the electron-ion equipartition heating power [35], which results in higher electron heating power even under the same ECRH power and transport conditions. Second, the pressure gradient becomes weak because of hollow density profile due to the neoclassical thermo-diffusion [11] induced by the higher  $T_e$ . Third, the heavier ion mass in the D plasma decreases  $\gamma_{RI}$ . All these effects result in the lower  $\gamma_{RI}$  in the D plasma. Particularly, low resistivity and heavier ion mass in the D plasma play the most important role in reducing  $\gamma_{RI}$ . In addition to the linear growth rate, the real frequency of RI turbulence is in the e-dia. direction [32], which is consistent with the experimental observation in the laboratory frame. These simulation results provide further evidence that the dominant turbulence is RI turbulence at  $\bar{n}_e > n_{tr}$ . Based on the above experimental and theoretical identification studies, the turbulence at  $\bar{n}_e < n_{tr}$  is identified as ITG turbulence, and that at  $\bar{n}_e > n_{tr}$  is identified as RI turbulence. The transition to RI turbulence in the high-density regime results in a reduction in the turbulence level in the D plasma, and it is the main cause of the improved confinement of the D plasma in ECRH plasmas on LHD.

In this study, a transition in the ion-scale turbulence was discovered in ECRH plasmas on LHD. The turbulence level reaches a minimum at a specific density with increase of electron density. Then, the electron density dependence and the propagation direction are reversed above the specific density. In the high-density regime, turbulence level was suppressed in D plasmas than in H plasmas. Furthermore, anomalous energy transport shows a similar trend of turbulence level, indicating that the measured turbulence plays an important role in confinement characteristics. Detailed turbulence measurements and simulations have identified that turbulence switches from ITG to RI turbulences below and above the specific density. Furthermore, the suppression of turbulence in high-density D plasmas was found to be due to weaker driving forces of RI, such as heavy ion mass and low resistivity. This reduction

mechanism is completely new and different from other core-isotope physics mechanisms, including the positive-mass effects of collisional stabilization of TEM [36,37],  $E \times B$  shear effect [38], and nonadiabatic electron effects of parallel motion [39]. Therefore, the observed turbulent transition provides new insights into isotope effects.

These findings are also essential for the operation and optimization of stellarators and heliotrons with reduced turbulence-driven anomalous transport. In a future stellarator and heliotron-type reactor,  $n_e \simeq 3 \times 10^{20} \text{ m}^{-3}$  and  $T_e = T_i \simeq 8 \text{ keV}$  in the core region are assumed as the condition to achieve  $Q = 10$  [40,41]. Under this assumption, the normalized collisionality ( $\nu_h^*$ ,  $\nu_h^* = 1$  corresponds to a boundary between  $1/\nu$  regime and plateau regime [11]) is approximately 7 at  $\rho = 0.5\text{--}0.7$ . This collisionality corresponds to the high-density RI region of  $n_e = 3.5 \times 10^{19} \text{ m}^{-3}$  for the H plasma and  $n_e = 4.0 \times 10^{19} \text{ m}^{-3}$  for the D plasma in our series of experiment. Currently, the operational limits of the high-temperature side are determined by neoclassical transport, whereas those of the high-density side are determined by radiation collapse [41]. Our study suggests that confinement degradation due to RI turbulence may also limit the operational regime on the high-density side. Therefore, concerning the configuration optimization to reduce anomalous transport, the magnetic-hill condition should be avoided to prevent confinement degradation by RI. However, if operation can be maintained at a minimum turbulence level at turbulence transition even under magnetic-hill conditions, confinement degradation can be prevented.

The data supporting the findings of this study are available in the LHD experiment data repository at [42].

The authors would like to thank all the members of the LHD Experiment group for their excellent work. The GKV simulations were performed on the Plasma Simulator at NIFS. This work was supported by NIFS Grants (No. 18ULHH013, No. 19ULHH013, No. 20ULHH013, No. 21ULHH013, and No. 22ULHH013), JSPS Grants (No. 21J12314, No. 16H04620, and No. 21H04458) and the U.S. DOE under No. DE-SC0019007.

---

[1] J. Wesson and D.J. Campbell, *Tokamaks* (Oxford University Press, New York, 2011), Vol. 149.  
 [2] J. Rice, J. Citrin, N. M. Cao, P. H. Diamond, M. Greenwald, and B. A. Grierson, *Nucl. Fusion* **60**, 105001 (2020).  
 [3] C. Angioni, E. Fable, M. Greenwald, M. Maslov, A. G. Peeters, H. Takenaga, and H. Weisen, *Plasma Phys. Controlled Fusion* **51**, 124017 (2009).  
 [4] J. Rice *et al.*, *Phys. Rev. Lett.* **107**, 265001 (2011).  
 [5] M. Osakabe *et al.*, *Nucl. Fusion* **62**, 042019 (2022).  
 [6] A. Dinklage *et al.*, *Nat. Phys.* **14**, 855 (2018).  
 [7] C. Beidler *et al.*, *Nucl. Fusion* **51**, 076001 (2011).

[8] F. Warmer *et al.*, *Phys. Rev. Lett.* **127**, 225001 (2021).  
 [9] K. Tanaka *et al.*, *Nucl. Fusion* **59**, 126040 (2019).  
 [10] K. Tanaka *et al.*, *Plasma Phys. Controlled Fusion* **62**, 024006 (2019).  
 [11] K. Tanaka *et al.*, *Fusion Sci. Technol.* **58**, 70 (2010).  
 [12] M. Nunami, T.-H. Watanabe, H. Sugama, and K. Tanaka, *Plasma Fusion Res.* **6**, 1403001 (2011).  
 [13] M. Nunami, T.-H. Watanabe, H. Sugama, and K. Tanaka, *Phys. Plasmas* **19** (2012).  
 [14] A. Ishizawa, T.-H. Watanabe, H. Sugama, M. Nunami, K. Tanaka, S. Maeyama, and N. Nakajima, *Nucl. Fusion* **55**, 043024 (2015).  
 [15] K. Tanaka *et al.*, *Nucl. Fusion* **57**, 116005 (2017).  
 [16] S. Sakakibara *et al.*, *Plasma Phys. Controlled Fusion* **50**, 124014 (2008).  
 [17] A. Glasser, J. Greene, and J. Johnson, *Phys. Fluids* **18**, 875 (1975).  
 [18] S. Sakakibara *et al.*, *Nucl. Fusion* **55**, 083020 (2015).  
 [19] K. Watanabe, S. Masamune, Y. Takemura, H. Funaba, S. Sakakibara, F. Watanabe, K. Tanaka, S. Ohdachi, K. Toi, and Y. Narushima, *Phys. Plasmas* **18**, 056119 (2011).  
 [20] C. Michael *et al.*, *Plasma Fusion Res.* **3**, S1071 (2008).  
 [21] H. Yamada *et al.*, *Nucl. Fusion* **45**, 1684 (2005).  
 [22] K. Tanaka, C. A. Michael, L. N. Vyacheslavov, A. L. Sanin, K. Kawahata, T. Akiyama, T. Tokuzawa, and S. Okajima, *Rev. Sci. Instrum.* **79**, 10E702 (2008).  
 [23] C. Michael, K. Tanaka, L. Vyacheslavov, A. Sanin, and K. Kawahata, *Rev. Sci. Instrum.* **86**, 093503 (2015).  
 [24] T. Kinoshita, K. Tanaka, H. Sakai, R. Yanai, M. Nunami, and C. A. Michael, *J. Instrum.* **18**, C11009 (2023).  
 [25] C. Suzuki *et al.*, *Plasma Phys. Controlled Fusion* **55**, 014016 (2012).  
 [26] T. I. Tsujimura *et al.*, *Nucl. Fusion* **55**, 123019 (2015).  
 [27] M. Yokoyama *et al.*, *Nucl. Fusion* **57**, 126016 (2017).  
 [28] C. Beidler and W. N. Hitchon, *Plasma Phys. Controlled Fusion* **36**, 317 (1994).  
 [29] T.-H. Watanabe and H. Sugama, *Nucl. Fusion* **46**, 24 (2005).  
 [30] M. Nunami, M. Nakata, S. Toda, and H. Sugama, *Phys. Plasmas* **27**, 052501 (2020).  
 [31] A. Ishizawa, D. Urano, Y. Nakamura, S. Maeyama, and T.-H. Watanabe, *Phys. Rev. Lett.* **123**, 025003 (2019).  
 [32] M. Sato and A. Ishizawa, *Phys. Plasmas* **24**, 082501 (2017).  
 [33] A. Ishizawa and N. Nakajima, *Phys. Plasmas* **14**, 040702 (2007).  
 [34] B. Carreras, V. Lynch, L. Garcia, and P. Diamond, *Phys. Fluids B* **5**, 1491 (1993).  
 [35] P. Schneider *et al.*, *Nucl. Fusion* **57**, 066003 (2017).  
 [36] M. Nakata, M. Nunami, H. Sugama, and T.-H. Watanabe, *Plasma Phys. Controlled Fusion* **58**, 074008 (2016).  
 [37] M. Nakata, M. Nunami, H. Sugama, and T.-H. Watanabe, *Phys. Rev. Lett.* **118**, 165002 (2017).  
 [38] J. Garcia, T. Görler, F. Jenko, and G. Giruzzi, *Nucl. Fusion* **57**, 014007 (2016).  
 [39] E. A. Belli, J. Candy, and R. E. Waltz, *Phys. Rev. Lett.* **125**, 015001 (2020).  
 [40] T. Goto *et al.*, *Plasma Phys. Controlled Fusion* **60**, 074001 (2018).  
 [41] T. Goto *et al.*, *Nucl. Fusion* **59**, 076030 (2019).  
 [42] [https://www-lhd.nifs.ac.jp/pub/Repository\\_en.html](https://www-lhd.nifs.ac.jp/pub/Repository_en.html).